Macedonian Journal of Chemistry and Chemical Engineering, Vol. **44**, No. 2, pp. 229–240 (2025)

MJCCA9 –

ISSN 1857-5552
e-ISSN 1857-5625

Received: October 28, 2025
Accepted: November 10, 2025

DOI: 10.20450/mjcce.2025.3334
Original scientific paper

FABRICATION AND CHARACTERIZATION OF ELECTROSPUN PLA/TUFF COMPOSITE MEMBRANES AS POTENTIAL ECO-FRIENDLY METAL ADSORBENTS

Aleksandra Ivanoska-Dacikj[1,2*], Gordana Bogoeva-Gaceva[1,3], Petre Makreski[4], Maja Ristova Delipetrev[2], Blažo Boev[1,2], Gligor Jovanovski[1,4]

[1]Research Centre for Environment and Materials, Macedonian Academy of Sciences and Arts, Krste Misirkov 2, 1000 Skopje, North Macedonia
[2]University "Goce Delčev" in Štip, Krste Misirkov 10-A, 2000 Štip, North Macedonia
[3]Faculty of Technology and Metallurgy, Ss. Cyril and Methodius University in Skopje, Rugjer Bošković 16, 1000 Skopje, North Macedonia
[4]Institute of Chemistry, Faculty of Natural Sciences and Mathematics, Ss. Cyril and Methodius University in Skopje, Arhimedova 5, 1000 Skopje, North Macedonia
aivanoska@manu.edu.mk

In this study, electrospinning was successfully employed to fabricate membranes based on polylactic acid (PLA), a polymer known for its biodegradability, containing varying amounts of opalized tuff (0, 2, 5, and 10 wt%). The addition of tuff introduced active mineral sites within the fibrous network, while the PLA matrix ensured mechanical stability, environmental sustainability, and prevention of secondary pollution. The electrospun membranes exhibited a uniform fibrous morphology with well-developed surface porosity, as confirmed by scanning electron microscopy. X-ray powder diffraction and Fourier-transform infrared spectroscopy verified the preservation of the characteristic structural features of both PLA and tuff, indicating successful incorporation of the filler without chemical alteration of the polymer matrix. Scanning electron microscopy combined with energy dispersive X-ray spectroscopy analysis demonstrated effective adsorption of nickel (Ni^{2+}) and lead (Pb^{2+}) ions from aqueous solutions, attributed to the high surface activity of the silicate mineral phase. These findings highlight the synergistic combination of a renewable, environmentally friendly polymer and a naturally occurring mineral filler to produce efficient and eco-friendly adsorptive membranes for heavy metal removal from aqueous solution.

Keywords: electrospinning; polylactic acid (PLA); opalized tuff; heavy metal adsorption; biodegradable composites.

ЕЛЕКТРОФОРМИРАЊЕ КОМПОЗИТНИ МЕМБРАНИ ОД PLA/ТУФ И НИВНА КАРАКТЕРИЗАЦИЈА КАКО ПОТЕНЦИЈАЛНИ АТСОРБЕНТИ ЗА МЕТАЛИ

Во овој труд успешно беше применета постапката на електроформирање за добивање мембрани од полимлечна киселина (PLA), добро познат биоразградлив полимер, со додаток на различни количини опализиран туф. Со внесувањето на туфот во полимерната фиброзна мембрана се создаваат активни минерални центри, додека полимерната матрица обезбедува механичка стабилност, еколошка одржливост и спречува секундарно загадување. Испитувањата со скенирачка електронска микроскопија покажаа дека добиените мембрани имаат рамномерна фиброзна морфологија со добро изразена површинска порозност. Анализите со рендгенска дифракција и FTIR-спектроскопија потврдија дека структурните својства на полимерот и на туфот се задржани и во композитните мембрани, што укажува на успешно вградување на полнилото без предизвикување хемиски интеракции со PLA. Како резултат на високата површинска активност на силикатната минерална фаза, мембраните покажаа ефикасни атсорпциони својства спрема јоните на никел (Ni^{2+}) и олово (Pb^{2+}), што беше потврдено со комбинираната анализа со скенирачка

електронска микроскопија и EDX. Добиените резултати покажуваат дека синергетската комбинација на еколошки полимер и природно минерално полнило овозможува добивање ефикасни и еко-одржливи атсорбенти за отстранување тешки метали од водни раствори.

Клучни зборови: електроформирање, полимлечна киселина (PLA), опализиран туф, атсорпција на тешки метали, биоразградливи композити

1. INTRODUCTION

Heavy metal contamination of water resources, especially from industrial discharges, represents a severe environmental and health risk.[1] Lead (Pb(II)), chromium (Cr(III)), cadmium (Cd(II)), and nickel (Ni(II)) are particularly hazardous due to their toxicity, persistence, and tendency to bioaccumulate.[2] Pb(II) is associated with neurological and developmental disorders, Cr(III) compounds are carcinogenic, Cd(II) causes kidney and bone damage, and Ni(II) induces systemic toxicity.[3] Therefore, it is essential to develop effective and sustainable methods for their removal from contaminated water.[3,4]

Compared with ion exchange, membrane separation, or chemical precipitation, adsorption is considered to be a more effective and economical strategy for heavy metal removal.[5,6] Traditional adsorbents such as activated carbon, clay minerals, and zeolites provide good uptake but are difficult to separate and regenerate, and often risk secondary pollution.[7–9] Embedding these materials in polymer membranes addresses these issues by stabilizing the adsorbent, preventing particle leaching, and improving accessibility of active sites.[10,11]

Electrospinning has emerged as a versatile method for producing nanofibrous membranes with fiber diameters in the submicron to micrometer range.[12–15] The resulting mats are highly porous and have a large surface area, enabling rapid mass transfer and efficient adsorption.[16,17] When combined with suitable fillers, electrospun membranes can act as multifunctional platforms for wastewater treatment.[18,19] Polylactic acid (PLA) is an attractive polymer for such applications due to its biodegradability, mechanical stability, and derivation from renewable resources.[20] Its use ensures environmental safety during both service and disposal, while providing compatibility with various inorganic additives.[21]

Opalized tuff, a volcanic rock composed mainly of hydrated amorphous silica and aluminosilicates, has demonstrated ion-exchange capacity, a high surface area, and an affinity for heavy metals.[22–24] However, its direct use can result in secondary pollution if particles are released into treated water. Incorporating tuff into electrospun PLA membranes combines the mineral's adsorption properties with the structural integrity and environmental sustainability of PLA, yielding hybrid membranes with improved performance and reduced environmental impact.

In this study, PLA-based electrospun membranes containing 0, 2, 5, and 10 wt% opalized tuff were fabricated and systematically characterized to evaluate the influence of mineral loading on morphology, structure, and adsorption performance. The incorporation of opalized tuff was expected to enhance the adsorption capacity of the membranes by introducing active silanol and aluminosilicate sites, while maintaining the mechanical integrity of the PLA matrix and its potential for biodegradability, as reported in previous studies. The membranes were characterized using scanning electron microscopy with energy-dispersive X-ray spectroscopy (SEM–EDX) to assess fiber morphology and to confirm mineral incorporation and metal adsorption. Additionally, X-ray powder diffraction (XRPD) and Fourier – transform infrared (FTIR) spectroscopy were employed to evaluate structural and compositional features. Adsorption tests were performed using aqueous solutions of Pb^{2+}, Ni^{2+}, Cd^{2+}, and Cr^{3+} ions to determine the affinity of the electrospun membranes toward different heavy metals.

2. MATERIALS AND METHODS

2.1. *Materials*

The PLA used in this study was provided by Esun (China), with a number-average molecular weight (M_n) of 60,520, a weight-average molecular weight (M_w) of 160,780, and a polydispersity (Q) of 2.6 (determined using gel permeation chromatography). The white opalized tuff with a primary particle size of 40 μm and a specific surface area of 39.3 $m^2\ g^{-1}$ was obtained as an industrial product from the mining company AD Strmoš (Probištip, North Macedonia) and subsequently processed at the company Nemetali Češinovo (North Macedonia). Opalized tuff is classified as a pyroclastic rock. It is lightweight, highly hydroscop-

ic, brittle, and friable, exhibiting high porosity and notable thermal stability. It is composed of the minerals tridymite, cristobalite, quartz, feldspar, and limonite. The chemical composition of the opalized tuff is presented in Table 1.[23–25] Chloroform, with the commercial name Chromasolv®, amylene stabilized, was purchased from Sigma-Aldrich.

T a b l e 1

Average chemical composition of white opalized tuff[25]

Chemical composition	wt%
SiO_2	94.51
Al_2O_3	3.04
Fe_2O_3	0.42
CaO	0.25
MgO	0.07
TiO_2	0.06
K_2O	0.13
Na_2O	0.25
Loss of ignition	1.43

2.2. *Sample preparation*

2.2.1. *Preparation of the polymer solutions*

PLA solutions (9 wt%) were prepared in chloroform with the addition of varying amounts of opalized white tuff (2, 5, and 10 wt% relative to the polymer). The control solution (without tuff) was obtained by dissolving 1 g of PLA in 10 g of chloroform, followed by homogenization by magnetic stirring at 200 rpm for 20 h at 25 °C using a hot plate (Witeg, Germany).

For the solutions containing opalized white tuff, 1 g of PLA was dissolved in 7 g of chloroform and homogenized at 25 °C on a magnetic stirrer overnight. The required amounts of tuff (0.02, 0.05, and 0.10 g) were separately dispersed in 3 g of chloroform using an ultrasonic bath at a frequency of 45 kHz for 10 min. The resulting tuff dispersion was then added to the pre-homogenized polymer solution. The polymer solutions with incorporated filler were further homogenized for 2 h at 25 °C on a magnetic stirrer.

Prior to electrospinning, all PLA/tuff solutions were sonicated for another 5 min in an ultrasonic bath to ensure uniform dispersion of the filler.

2.2.2. *Samples preparation by electrospinning*

Electrospinning was performed using the E-Fiber EF100 System (SKE Technologies, Italy). The polymer solution was loaded into a 10 ml syringe with a stainless-steel blunt needle (inner diameter: 0.6 mm; outer diameter: 0.91 mm) and mounted onto a syringe pump. A rotating drum collector covered with aluminum foil was used to collect the fibers. A high voltage (15 kV) was applied to the needle, while the drum was grounded. The distance between the needle tip and the collector was maintained at 12 cm. Electrospinning was conducted at a flow rate of 2 ml/h, a collector rotation speed of 300 rpm, a temperature of 25 °C, and a relative humidity of 40 %. The electrospinning parameters were selected based on preliminary optimization experiments to ensure the formation of uniform, bead-free fibers. Following this process, four distinct samples were obtained, designated PLA-TUFF-0, PLA-TUFF-2, PLA-TUFF-5, and PLA-TUFF-10, corresponding to the different tuff loadings. Figure 1 shows a schematic representation of the electrospinning setup used for sample fabrication.

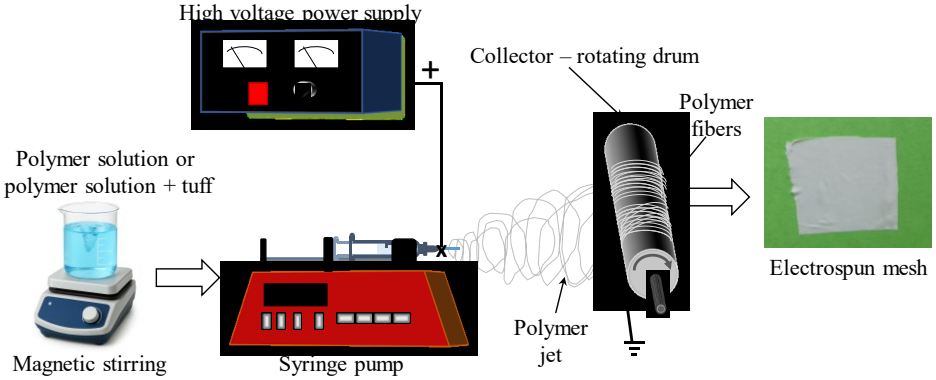

Fig. 1. A schematic illustration of the electrospinning process for sample fabrication

2.2.3. *Preparation of metal ion solutions and the adsorption procedure*

The ability of the electrospun membranes to adsorb selected metal ions from aqueous solutions was evaluated in controlled adsorption experiments. Single-component aqueous solutions of the following metal ions were prepared: Pb^{2+}, Cr^{3+}, Cd^{2+}, and Ni^{2+}, with concentrations of 600, 120, 50, and 250 μg l^{-1}, respectively. The selected concentrations were based on toxicity levels reported in previous studies.[22] The pH of the Pb^{2+}, Cr^{3+}, Cd^{2+}, and Ni^{2+} aqueous solutions was measured prior to the adsorption experiments; it was 6.2, 6.5, 5.9, and 6.0, respectively. Accurately weighed membrane samples (10 mg each) were immersed in 70 ml of the metal ion solutions at room temperature and subjected to agitation using a horizontal bench shaker to ensure uniform contact. After exposure for 6 h, the membranes were removed, thoroughly rinsed with deionized water to eliminate residual ions, and dried under ambient conditions. The dried samples were subsequently examined with SEM–EDX to evaluate surface morphology and confirm metal ion adsorption.

2.3. *Methods of characterisation*

2.3.1. *SEM–EDX*

SEM and EDX analyses were conducted to examine the surface morphology, structural uniformity, and elemental composition of the electrospun PLA/tuff fibers. The morphology of the electrospun fibers was evaluated using a VEGA3 LMU scanning electron microscope (Tescan, Czech Republic), equipped with an EDX system with a silicon drift detector (SDD). The samples were mounted to the holder using double-stick carbon tape, and the specimens were coated with a layer of gold (5 nm) using a sputter coater (Q150R ES, Quorum Technologies Ltd, UK). Prepared samples were placed into the chamber with a five axes (*x*, *y*, *z*, rotation, and tilt) motorized stage and analyzed using 10 keV acceleration voltage and high-vacuum mode (≤ 0.018 Pa). The average fiber diameters were determined by measuring 30 randomly selected fibers at three different locations on each sample, resulting in a total of 90 measurements per sample. SEM–EDX spectra were acquired from specific points on the micrographs where metal particles or surface deposits were visible, to confirm the localized adsorption of metal ions on the membrane surface.

2.3.2. *FTIR spectroscopy*

FTIR spectroscopy was used to identify the characteristic functional groups and to examine the possible interactions between PLA and tuff in the composite fibers. FTIR spectra were recorded using a Cary 630 FTIR spectrometer (Agilent, USA) equipped with a diamond attenuated total reflectance (ATR) accessory. Spectral acquisition was performed over the range of 4000–500 cm^{-1} with a spectral resolution of 2 cm^{-1}. Each spectrum represents the average of 32 co-added scans to improve the signal-to-noise ratio. Peak deconvolution and curve fitting (using Gaussian function with a linear baseline) were performed using Grams AI™ Spectroscopy Software.

2.3.3. *XRPD*

XRPD analysis was conducted to assess the crystalline structure and phase composition of the composite fibers. XRPD patterns were recorded on an Ultima IV diffractometer (Rigaku, Japan) equipped by a high-speed position-sensitive linear (1D) D/teX Ultra detector. The X-ray beam was Ni-filtered Cu*K*α (λ = 0.154178 nm), and the radiation was generated by setting the tube voltage at 40 kV and the tube current to 40 mA. The following optical components were used: a 2/3° divergence slit, a 10 mm divergence height slit, and an 8 mm scattering slit. Diffraction data were collected over a 2θ range from 5º to 70º at a constant scanning rate of 5°/min.

3. RESULTS AND DISCUSSION

3.1. *Morphology of the electrospun PLA/tuff fibers*

SEM micrographs of the electrospun fibers reveal clear morphological features as a function of opalized tuff loading (Fig. 2). The neat PLA fibers (PLA-TUFF-0) display a relatively smooth surface and uniform cylindrical morphology, with an average fiber diameter of 5.92 ± 2.21 μm. The fibrous mat is randomly oriented and shows no evidence of bead formation, confirming the stability of the electrospinning process under the chosen conditions.

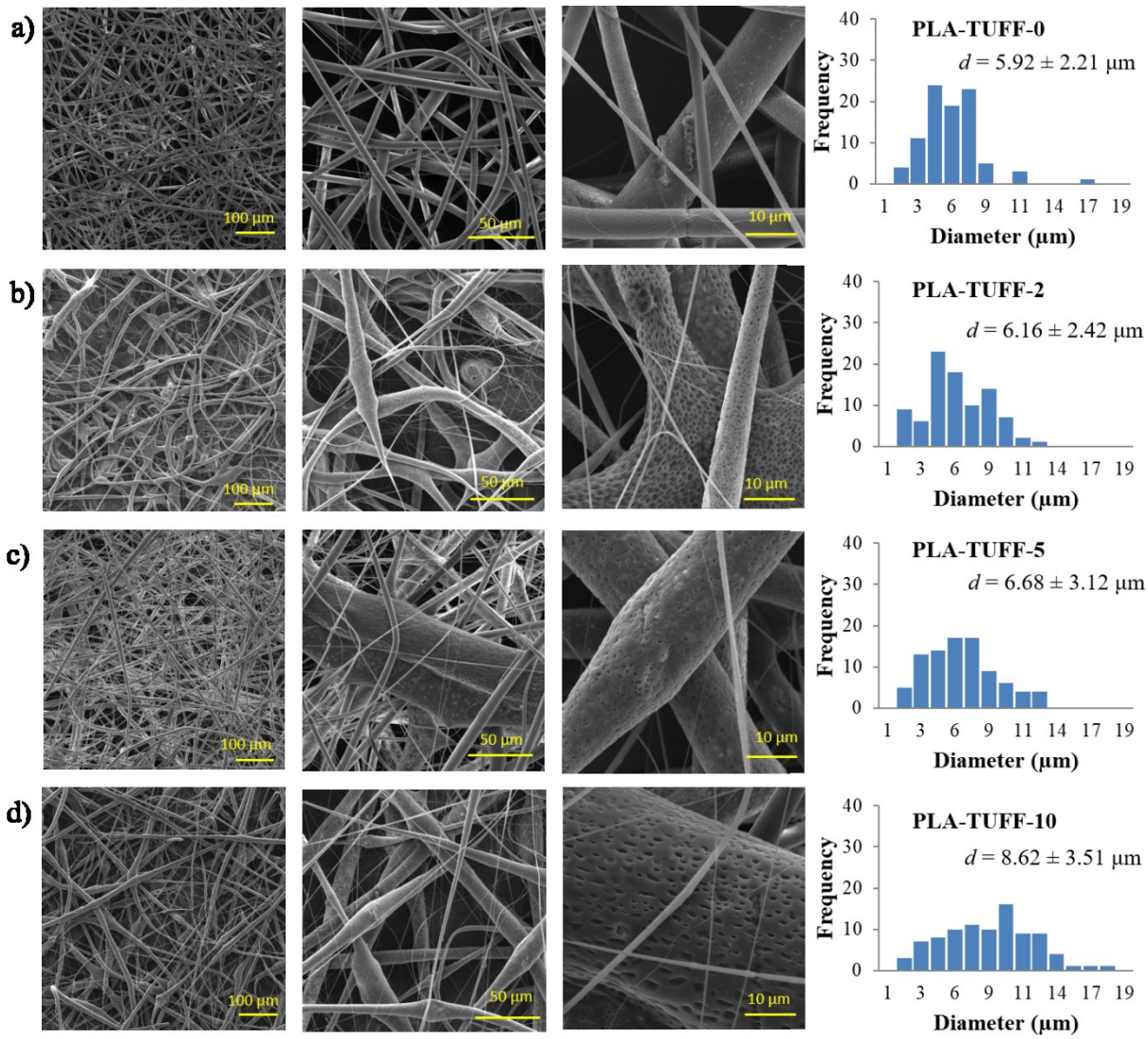

Fig. 2. SEM micrographs at different magnifications and the corresponding fiber diameter distributions of the PLA/tuff electrospun membranes: (a) PLA-TUFF-0, (b) PLA-TUFF-2, (c) PLA-TUFF-5, and (d) PLA-TUFF-10

Incorporation of 2 wt% tuff (PLA-TUFF-2) induces noticeable morphological changes. The fibers exhibit a rougher surface texture, discrete pores appear along the fiber length, and a predominantly continuous fibrous network is maintained. The pore formation is likely related to phase separation phenomena and rapid solvent evaporation, promoted by the presence of inorganic particles that modify the solution conductivity and jet solidification dynamics.[26–28] The average diameter increases slightly to 6.16 ± 2.42 µm, but the distribution broadens, suggesting heterogeneity introduced by the mineral filler.

With 5 wt% tuff loading (PLA-TUFF-5), the porous structure becomes significantly more pronounced, with many fibers displaying uniformly distributed nanoscale to submicron pores on their surfaces. Such a "breath figure" morphology (characterized by nanoscale pores formed via condensation of water droplets during solvent evaporation) is often associated with solvent–nonsolvent exchange and vapor-induced phase separation during electrospinning.[29–31] The increased filler content appears to enhance this effect, possibly by acting as nucleation sites for pore formation. Fiber diameters further increase (6.68 ± 3.12 µm) and the diameter distribution broadens, reflecting reduced jet stability at higher mineral loadings. Nevertheless, the fibrous network remains interconnected, indicating good spinnability of PLA even in the presence of a substantial amount of inorganic filler.

At the highest tuff concentration (PLA-TUFF-10), the fibers show the largest average diameter (8.62 ± 3.51 µm), accompanied by a wide distribution and increased structural heterogeneity. The porous character of the fibers is particularly evident at this loading, with well-developed surface porosity contributing to a highly porous over-

all membrane architecture. This high porosity is expected to be beneficial for adsorption applications, as it increases the accessible surface area and facilitates mass transfer within the fibrous network.

Overall, the addition of opalized tuff promotes pore nucleation and increases fiber roughness without compromising structural integrity. The observed porosity arises from the combined effects of enhanced conductivity and localized phase separation during solvent evaporation, consistent with reports on PLA composites containing silica and mineral fillers.[32,33] These morphological features make the PLA/tuff membranes well-suited for applications requiring high permeability and a large active surface area, such as heavy metal adsorption.

3.2. *XRPD analysis*

The XRPD spectrum of the opalized tuff (Fig. 3) reveals a multiphase mineralogical composition dominated by silica polymorphs. The most intense reflections are attributed to tridymite, with characteristic peaks observed at 2θ = 21.6°, 20.5°, and 35.9°, consistent with standard references for these silica polymorphs.[34,35] Cristobalite is also detected, with reflection at 2θ = 22.0°, overlapping with that of tridymite but distinguishable by its slightly shifted position.[36] A sharp and well-defined peak at 2θ = 26.6°, along with secondary reflections at 2θ = 20.8° and 50.1°, corresponds to α-quartz, confirming the presence of stable crystalline silica domains.[37]

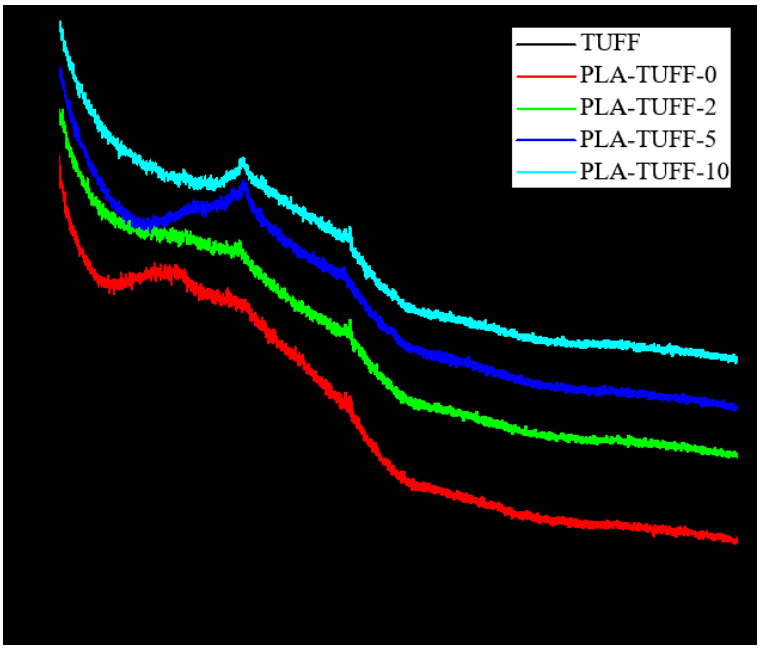

Fig. 3. The XRPD patterns of opalized tuff and the PLA/tuff electrospun membranes with varying filler contents

Peak deconvolution and curve fitting were carried out to resolve the overlapping diffraction reflections of tridymite, cristobalite, and α-quartz (Fig. 4). The analysis was performed in the 2θ range of 20°–23°, resulting in the identification and separation of three distinct peaks with maxima at 20.7° (α-quartz), 21.7° (tridymite), and 21.9° (cristobalite). The fitting quality is high, with a correlation coefficient (R^2) of 0.990, confirming the reliability of the deconvolution. This result highlights the multiphase siliceous nature of opalized tuff, consistent with previous reports on volcanic-derived silica polymorphs.[38,39] The presence of surface silanol groups (Si–OH) and aluminosilicates is expected to enhance metal ion binding via ion exchange and complexation.

The XRPD patterns of the electrospun PLA and PLA/tuff membranes show that the polymer retains its broad amorphous halo centered at 2θ ≈ 16°–19° (Fig. 3), typical of the α-form of PLA with low crystallinity.[40,41] The absence of sharp reflections confirms that electrospinning favors the formation of an amorphous or poorly ordered PLA structure, in agreement with previous studies on electrospun biopolymer fibers.[42,43]

Weak reflections near 2θ = 22.5° (Fig. 3) appear in the composites, corresponding to the crystalline tuff phases.[34–37] The intensity of this peak becomes more pronounced as the filler content increases, confirming the successful incorporation and the rising contribution of the mineral phase within the PLA matrix.

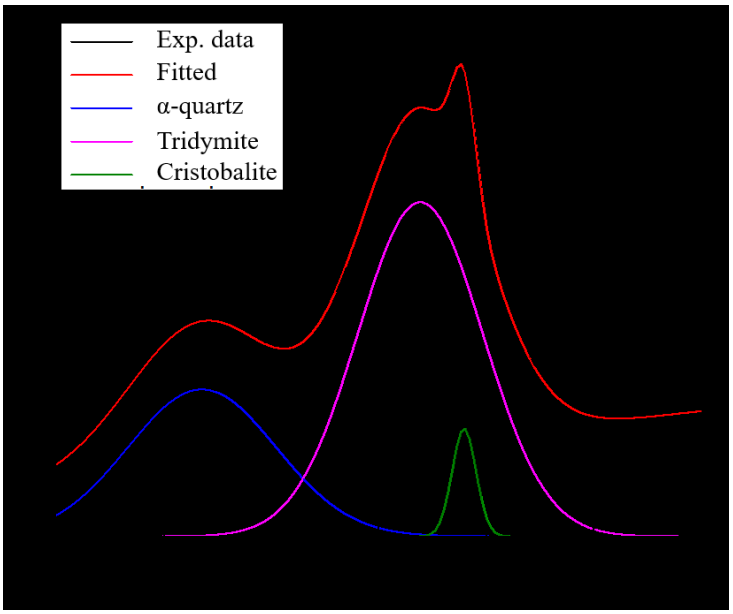

Fig. 4. Peak deconvolution of the XRPD spectrum of opalized tuff in the 2θ range of 20°–23°, showing resolved contribution bands from α-quartz, tridymite, and cristobalite.

Importantly, the incorporation of tuff does not significantly alter the crystallinity of the PLA matrix itself. Instead, the results indicate a composite structure in which the amorphous polymer phase coexists with dispersed crystalline mineral domains. This composite structure (PLA/TUFF) increases the availability of active adsorption sites and, consequently, improves the adsorption performance, without affecting the structural characteristics of PLA, which is known for its biodegradability.

3.3. *FTIR spectroscopy analysis*

The FTIR spectrum of opalized tuff (Fig. 5) shows characteristic silicate vibrations for quartz, tridymite, and cristobalite: a strong Si–O–Si asymmetric stretch represented by band at ~1080 cm^{-1} and a symmetric stretch manifested by band near 790 cm^{-1}.[44–46] The absence of bands in the 3600–3700 cm^{-1} region indicates minimal hydroxylation, consistent with a dehydrated siliceous structure.

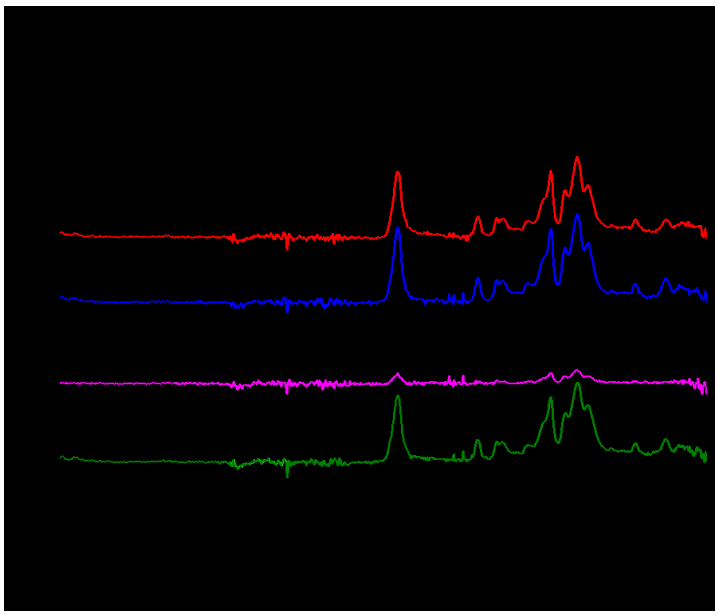

Fig. 5. The FTIR spectra of opalized tuff and the PLA/tuff electrospun membranes with varying filler contents

Neat PLA (PLA-TUFF-0) shows its characteristic vibrational profile: a strong C=O stretching band at ~1750 cm^{-1}, C–O–C and C–O stretching bands between 1180 and 1080 cm^{-1}, and CH_3 stretching and bending bands at 2995 and 1450–1380 cm^{-1}, respectively.[44,45] These features dominate the spectra of all composites regardless of the filler loading, confirming that the PLA backbone remains intact after electrospinning and mineral incorporation.

In the composite membranes (2, 5, and 10 wt% tuff), the PLA signals largely mask the tuff contributions, because the Si–O bands of the filler overlap with the region of polymer spectral C–O stretching bands. As a result, no systematic changes with increasing tuff concentration can be resolved in the FTIR spectra. This indicates that the mineral is physically embedded in the fibrous matrix without generating new covalent bonding, as corroborated by the XRPD results.

3.4. *SEM–EDX analysis*

The adsorption of metal ions onto the electrospun membranes was investigated using SEM–EDX after immersing the PLA-TUFF-0 and PLA-TUFF-10 membranes in individual aqueous metal ion solutions of Pb^{2+}, Ni^{2+}, Cd^{2+}, and Cr^{3+} for 6 h. The SEM–EDX analysis revealed detectable metal adsorption only for Pb^{2+} and Ni^{2+}, and exclusively for the PLA-TUFF-10 membrane. Thus, SEM micrographs are presented only for exposure to Pb^{2+} and Ni^{2+}, showing both the PLA-TUFF-0 and PLA-TUFF-10 membranes, together with the EDX spectra and elemental composition tables for PLA-TUFF-10, which confirmed the presence of Pb and Ni (Fig. 6).

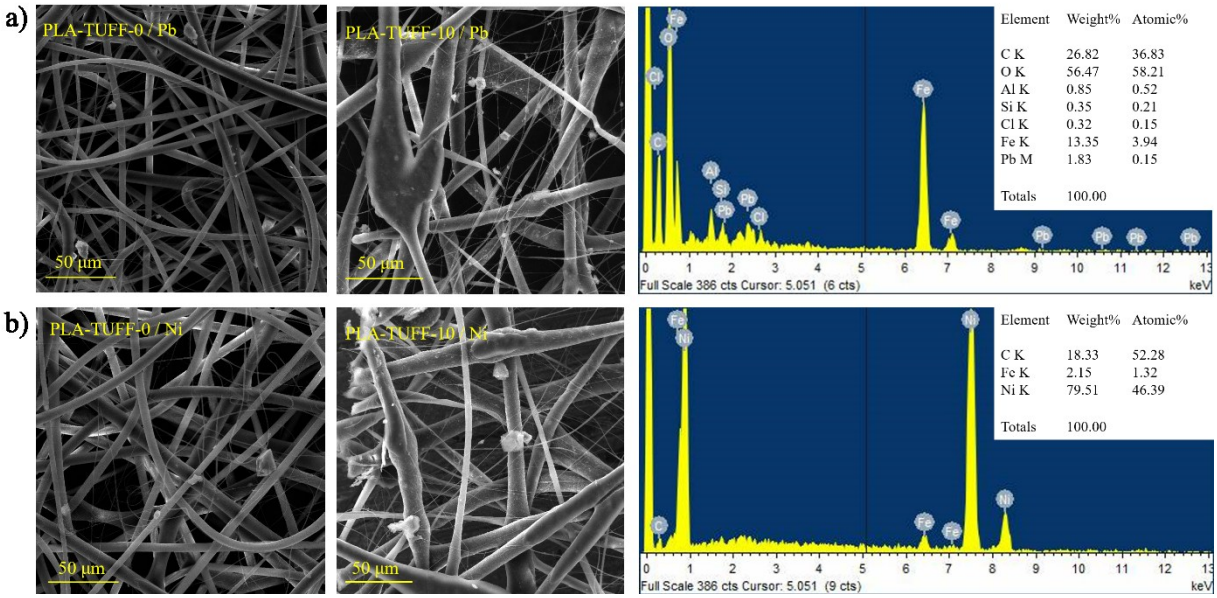

Fig. 6. SEM–EDX analysis of the electrospun PLA-TUFF-0 and PLA-TUFF-10 membranes after exposure to Pb^{2+} and Ni^{2+} solutions for 6 h. (**a**) Pb^{2+} solution: from left to right – micrographs of the PLA-TUFF-0 and PLA-TUFF-10 membranes and the EDX spectrum and elemental composition table of PLA-TUFF-10 membrane, confirming the presence of Pb. (**b**) Ni^{2+} solution: from left to right – micrographs of the PLA-TUFF-0 and PLA-TUFF-10 membranes and the EDX spectrum and elemental composition table of PLA-TUFF-10, confirming the presence of Ni

The surface morphology of the PLA-TUFF-0 and PLA-TUFF-10 membranes exhibited distinct differences following metal exposure. After immersion in the Pb^{2+} solution, the PLA-TUFF-10 fibers showed visible surface deposits and agglomerates, while the PLA-TUFF-0 membrane remained smooth and unchanged. The corresponding EDX spectrum of the PLA-TUFF-10 membrane confirmed the presence of Pb, with a weight percentage of 1.83 wt%, along with Si, Al, Fe, and O peaks originating from the mineral filler. There was no Pb signal on the PLA-TUFF-0 membrane, indicating that the polymer itself has limited affinity for Pb^{2+} ions. The observed adsorption can therefore be attributed to the presence of active sites – particularly surface silanol (Si–OH) and aluminosilicate groups – introduced by the opalized tuff filler.[47]

There was a similar trend for the Ni^{2+} solution. Surface deposits were clearly visible on the

PLA-TUFF-10 membrane, while the PLA-TUFF-0 fibers showed no detectable changes. The EDX analysis revealed a strong Ni signal, corresponding to 79.5 wt% of the detected elements, demonstrating a substantially higher adsorption capacity compared to Pb^{2+}. The enhanced Ni^{2+} uptake can be ascribed to the smaller ionic radius of Ni^{2+} (0.69 Å)[48] and its higher charge density, which favor inner-sphere complexation with oxygen donor atoms on SiO_2 and Fe_2O_3 surfaces.[49,50] In contrast, Pb^{2+} ions (ionic radius 1.19 Å) exhibit weaker coordination with silicate surfaces and a greater tendency to form insoluble hydroxides ($Pb(OH)_2$) at near-neutral pH, which limits their availability for adsorption.[51,52]

For the Cd^{2+} and Cr^{3+} solutions, neither SEM nor EDX analyses revealed evidence of metal adsorption. The absence of Cd and Cr signals can be explained by their physicochemical properties. Cd^{2+}, with a larger ionic radius (0.97 Å) and higher hydration energy (−1800 kJ mol^{-1}), remains strongly hydrated in aqueous environments, hindering dehydration and surface complexation with silicate surfaces.[53,54] Cr^{3+} typically hydrolyzes to $Cr(OH)_2^+$ and $Cr(OH)_3$ at near-neutral pH, leading to low solubility and limited interaction with negatively charged silanol sites.[55,56] These effects collectively suppress the adsorption of Cd^{2+} and Cr^{3+} onto both neat and composite membranes.

Overall, the results confirm that embedding opalized tuff within the PLA matrix enhances the adsorption performance toward transition metal ions, particularly Ni^{2+} and Pb^{2+}. The high content of amorphous to microcrystalline silica and iron oxides in the tuff provides abundant active sites for metal binding through electrostatic attraction and surface complexation mechanisms.[57,58] Meanwhile, the PLA matrix ensures mechanical stability and processability, contributing to an efficient and environmentally sustainable adsorptive membrane system.[59]

4. CONCLUSIONS

This study demonstrated that incorporating opalized tuff into electrospun PLA membranes enhances their morphological and functional characteristics without altering the intrinsic structure of the polymer. The addition of tuff induces surface porosity and introduces active mineral sites that improve adsorption performance. Structural analyses (XRPD and FTIR spectroscopy) confirmed the coexistence of amorphous PLA and crystalline silica phases, while SEM–EDX revealed selective adsorption of Pb^{2+} and Ni^{2+} ions on the PLA-TUFF-10 membrane. In contrast, Cd^{2+} and Cr^{3+} showed minimal interaction, indicating selective adsorption governed by the properties of the metal ions and the membrane surface chemistry.

This study represents a promising preliminary investigation. Additional studies are needed to systematically investigate the influence of operational parameters, such as pH, contact time, temperature, and the initial ion concentration, on adsorption efficiency, and to explore adsorption kinetics, equilibrium behavior, and membrane reusability, to optimize the performance of PLA/TUFF composites for efficient and sustainable wastewater treatment applications.

REFERENCES

(1) Aziz, K. H. H.; Mustafa, F. S.; Omer, K. M.; Hama, S.; Hamarawf, R. F.; Rahman, K. O. Heavy Metal Pollution in the Aquatic Environment: Efficient and Low-Cost Removal Approaches to Eliminate Their Toxicity: A Review. *RSC Adv.* **2023**, *13* (26), 17595–17610. https://doi.org/10.1039/D3RA00723E

(2) Ali, H.; Khan, E.; Ilahi, I. Environmental Chemistry and Ecotoxicology of Hazardous Heavy Metals: Environmental Persistence, Toxicity, and Bioaccumulation. *J. Chem.* **2019**, *2019* (1), 6730305. https://doi.org/10.1155/2019/6730305

(3) Zhang, P.; Yang, M.; Lan, J.; Huang, Y.; Zhang, J.; Huang, S.; Yang, Y.; Ru, J. Water Quality Degradation Due to Heavy Metal Contamination: Health Impacts and Eco-Friendly Approaches for Heavy Metal Remediation. *Toxics* **2023**, *11* (10), 828. https://doi.org/10.3390/toxics11100828

(4) Singh, V.; Ahmed, G.; Vedika, S.; Kumar, P.; Chaturvedi, S. K.; Rai, S. N.; Vamanu, E.; Kumar, A. Toxic Heavy Metal Ions Contamination in Water and Their Sustainable Reduction by Eco-Friendly Methods: Isotherms, Thermodynamics and Kinetics Study. *Sci. Rep.* **2024**, *14* (1), 7595. https://doi.org/10.1038/s41598-024-58061-3

(5) Chai, W. S.; Cheun, J. Y.; Kumar, P. S.; Mubashir, M.; Majeed, Z.; Banat, F.; Ho, S.-H.; Show, P. L. A Review on Conventional and Novel Materials towards Heavy Metal Adsorption in Wastewater Treatment Application. *J. Clean. Prod.* **2021**, *296*, 126589. https://doi.org/10.1016/j.jclepro.2021.126589

(6) Rajendran, S.; Priya, A. K.; Senthil Kumar, P.; Hoang, T. K. A.; Sekar, K.; Chong, K. Y.; Khoo, K. S.; Ng, H. S.; Show, P. L. A Critical and Recent Developments on Adsorption Technique for Removal of Heavy Metals from Wastewater. A Review. *Chemosphere* **2022**, *303*, 135146. https://doi.org/10.1016/j.chemosphere.2022.135146

(7) Ali, I. The Quest for Active Carbon Adsorbent Substitutes: Inexpensive Adsorbents for Toxic Metal Ions Removal from Wastewater. *Sep. Purif. Rev.* **2010**, *39* (3–4), 95–171. https://doi.org/10.1080/15422119.2010.527802

(8) Akhtar, M. S.; Ali, S.; Zaman, W. Innovative Adsorbents for Pollutant Removal: Exploring the Latest Research and Applications. *Molecules* **2024**, *29* (18), 4317. https://doi.org/10.3390/molecules29184317

(9) Momina; Shahadat, M.; Isamil, S. Regeneration Performance of Clay-Based Adsorbents for the Removal of Industrial Dyes: A Review. *RSC Adv.* **2018**, *8* (43), 24571–24587. https://doi.org/10.1039/C8RA04290J

(10) Agboola, O.; Fayomi, O. S. I.; Ayodeji, A.; Ayeni, A. O.; Alagbe, E. E.; Sanni, S. E.; Okoro, E. E.; Moropeng, L.; Sadiku, R.; Kupolati, K. W.; Oni, B. A. A Review on Polymer Nanocomposites and Their Effective Applications in Membranes and Adsorbents for Water Treatment and Gas Separation. *Membranes* **2021**, *11* (2), 139. https://doi.org/10.3390/membranes11020139

(11) Vo, T. S.; Hossain, M. M.; Jeong, H. M.; Kim, K. Heavy Metal Removal Applications Using Adsorptive Membranes. *Nano Converg.* **2020**, *7* (1), 36. https://doi.org/10.1186/s40580-020-00245-4

(12) Ivanoska-Dacikj, A.; Bogoeva-Gaceva, G.; Krumme, A.; Tarasova, E.; Scalera, C.; Stojkovski, V.; Gjorgoski, I.; Ristoski, T. Biodegradable Polyurethane/Graphene Oxide Scaffolds for Soft Tissue Engineering: In Vivo Behavior Assessment. *Int. J. Polym. Mater. Polym. Biomater.* **2020**, *69* (17), 1101–1111. https://doi.org/10.1080/00914037.2019.1655754

(13) Ivanoska-Dacikj, A.; Makreski, P.; Bogoeva-Gaceva, G. Fabrication of Biodegradable Polyurethane Electrospun Webs of Fibers Modified with Biocompatible Graphene Oxide Nanofiller. *J. Ind. Text.* **2022**, *51* (3 suppl), 4041S-4065S. https://doi.org/10.1177/15280837211003165

(14) Ivanoska-Dacikj, A.; Makreski, P.; Sukumaran, S.; Stachewicz, U. Design of Experiments as a Comprehensive Framework to Optimize Electrospinning Parameters for Enhanced β-Phase in Poly(Vinylidene Fluoride-Co-Hexafluoropropylene). *J. Polym. Res.* **2025**, *32* (9), 303. https://doi.org/10.1007/s10965-025-04515-9

(15) Ivanoska-Dacikj, A.; Makreski, P.; Geskovski, N.; Karbowniczek, J.; Stachewicz, U.; Novkovski, N.; Tanasić, J.; Ristić, I.; Bogoeva-Gaceva, G. Electrospun PEO/rGO Scaffolds: The Influence of the Concentration of rGO on Overall Properties and Cytotoxicity. *Int. J. Mol. Sci.* **2022**, *23* (2), 988. https://doi.org/10.3390/ijms23020988

(16) Zheng, W.; Liu, Z.; Ding, R.; Dai, Y.; Li, X.; Ruan, X.; He, G. Constructing Continuous and Fast Transport Pathway by Highly Permeable Polymer Electrospun Fibers in Composite Membrane to Improve CO_2 Capture. *Sep. Purif. Technol.* **2022**, *285*, 120332. https://doi.org/10.1016/j.seppur.2021.120332

(17) Pereao, O. K.; Bode-Aluko, C.; Ndayambaje, G.; Fatoba, O.; Petrik, L. F. Electrospinning: Polymer Nanofibre Adsorbent Applications for Metal Ion Removal. *J. Polym. Environ.* **2017**, *25* (4), 1175–1189. https://doi.org/10.1007/s10924-016-0896-y

(18) Kumar, M.; Chowdhury, S.; Kaur Randhawa, J. Emerging Trends in Membrane-Based Wastewater Treatment: Electrospun Nanofibers and Reticular Porous Adsorbents as Key Components. *Environ. Sci. Water Res. Technol.* **2024**, *10* (1), 29–84. https://doi.org/10.1039/D3EW00119A

(19) Kumar, S.; Shandilya, M.; Uniyal, P.; Thakur, S.; Parihar, N. Efficacy of Polymeric Nanofibrous Membranes for Proficient Wastewater Treatment. *Polym. Bull.* **2023**, *80* (7), 7145–7200. https://doi.org/10.1007/s00289-022-04417-6

(20) Auras, R. A.; Lim, L.-T.; Selke, S. E. M.; Tsuji, H. *Poly(Lactic Acid): Synthesis, Structures, Properties, Processing, Applications, and End of Life*; John Wiley & Sons, 2022.

(21) Vidović, E.; Faraguna, F.; Jukić, A. Influence of Inorganic Fillers on PLA Crystallinity and Thermal Properties. *J. Therm. Anal. Calorim.* **2017**, *127* (1), 371–380. https://doi.org/10.1007/s10973-016-5750-x

(22) Zhao, S.; Li, Q.; Tang, Z.; Yang, Y.; Wu, J.; Gao, P.; Qian, Y.; Chen, J.; Xue, G. Simultaneous Removal of Cr, Cu, Zn, and Cd by Nano Zero-Valent Iron Modified Sludge Biochar in High Salinity Wastewater. *Sep. Purif. Technol.* **2024**, *347*, 127560. https://doi.org/10.1016/j.seppur.2024.127560

(23) Boškovski, B.; Bogoevski, S.; Ruseska, G.; Atkovska, K. High Temperature Crystallization Process into Opalized Tuff. *Geol. Maced.* **2015**, *29* (2), 209–213.

(24) Bogoevski, S.; Boškovski, B.; Ruseska, G.; Atkovska, K. Concentration of Carbonate Admixture from Opalized Tuff into One Separate Fraction; *Geol. Maced.* **2016**, *30* (1), 89–95.

(25) AD Strmoš Probištip – Macedonia. Opalized tuff — general, chemical, mineralogical, and physical properties. *Strmoš: Macedonia* (archived Oct 18, 2009). https://web.archive.org/web/20091018163225/http://www.strmos.com.mk/DesktopDefault.aspx?tabindex=1&tabid=23 (accessed Sept 16, 2025).

(26) Pervin, R.; Ghosh, P.; Basavaraj, M. G. Tailoring Pore Distribution in Polymer Films via Evaporation Induced Phase Separation. *RSC Adv.* **2019**, *9* (27), 15593–15605. https://doi.org/10.1039/C9RA01331H

(27) Chan, K.-Y.; Li, C.-L.; Wang, D.-M.; Lai, J.-Y. Formation of Porous Structures and Crystalline Phases in Poly(Vinylidene Fluoride) Membranes Prepared with Nonsolvent-Induced Phase Separation – Roles of Solvent Polarity. *Polymers* **2023**, *15* (5), 1314. https://doi.org/10.3390/polym15051314

(28) Faustini, M.; Boissière, C.; Nicole, L.; Grosso, D. From Chemical Solutions to Inorganic Nanostructured Materials: A Journey into Evaporation-Driven Processes. *Chem. Mater.* **2014**, *26* (1), 709–723. https://doi.org/10.1021/cm402132y

(29) Huang, C.; Thomas, N. L. Fabrication of Porous Fibers via Electrospinning: Strategies and Applications. *Polym. Rev.* **2020**, *60* (4), 595–647. https://doi.org/10.1080/15583724.2019.1688830

(30) Huang, X.; Gao, J.; Zheng, N.; Li, W.; Xue, H.; Li, R. K. Y. Influence of Humidity and Polymer Additives on the Morphology of Hierarchically Porous Microspheres Prepared from Non-Solvent Assisted Electrospraying. *Colloids Surf. Physicochem. Eng. Asp.* **2017**, *517*, 17–24. https://doi.org/10.1016/j.colsurfa.2017.01.003

(31) Natarajan, L.; New, J.; Dasari, A.; Yu, S.; Manan, M. A. Surface Morphology of Electrospun PLA Fibers: Mechanisms of Pore Formation. *RSC Adv.* **2014**, *4* (83), 44082–44088. https://doi.org/10.1039/C4RA06215A

(32) Jing, M.; Liu, X.; Ma, L.; Cao, F.; Wang, Z.; Wang, Y.; Liu, C.; Shen, C. Impact of the Topography of Fiber Surface on the Interfacial Crystallization Behavior of Poly(Lactide). *Macromolecules* **2023**, *56* (18), 7454–7466. https://doi.org/10.1021/acs.macromol.3c00014

(33) Rezabeigi, E.; Wood-Adams, P. M.; Demarquette, N. R. Complex Morphology Formation in Electrospinning of Binary and Ternary Poly(Lactic Acid) Solutions. *Macromolecules* **2018**, *51* (11), 4094–4107. https://doi.org/10.1021/acs.macromol.8b00083

(34) Eversull, L. G.; Ferrell, R. E. Disordered Silica with Tridymite-like Structure in the Twiggs Clay. *Am. Mineral.* **2008**, *93* (4), 565–572. https://doi.org/10.2138/am.2008.2603

(35) Elzea, J. M.; Rice, S. B. Tem and X-Ray Diffraction Evidence for Cristobalite and Tridymite Stacking Sequences in Opal. *Clays Clay Miner.* **1996**, *44* (4), 492–500. https://doi.org/10.1346/CCMN.1996.0440407

(36) Önal, M.; Kahraman, S.; Sarıkaya, Y. Differentiation of α-Cristobalite from Opals in Bentonites from Turkey. *Appl. Clay Sci.* **2007**, *35* (1), 25–30. https://doi.org/10.1016/j.clay.2006.07.003

(37) Beddiaf, S.; Chihi, S.; Leghrieb, Y. The Determination of Some Crystallographic Parameters of Quartz, in the Sand Dunes of Ouargla, Algeria. *J. Afr. Earth Sci.* **2015**, *106*, 129–133. https://doi.org/10.1016/j.jafrearsci.2015.03.014

(38) Martel, C.; Pichavant, M.; Di Carlo, I.; Champallier, R.; Wille, G.; Castro, J. M.; Devineau, K.; Davydova, V. O.; Kushnir, A. R. L. Experimental Constraints on the Crystallization of Silica Phases in Silicic Magmas. *J. Petrol.* **2021**, *62* (1), egab004. https://doi.org/10.1093/petrology/egab004

(39) Graetsch, H. Structural Characteristics of Opaline and Microcrystalline Silica Minerals. *Rev. Mineral. Geochem.* **1994**, *29* (1), 209–232.

(40) Oliveira, J. E.; Mattoso, L. H. C.; Orts, W. J.; Medeiros, E. S. Structural and Morphological Characterization of Micro and Nanofibers Produced by Electrospinning and Solution Blow Spinning: A Comparative Study. *Adv. Mater. Sci. Eng.* **2013**, *2013* (1), 409572. https://doi.org/10.1155/2013/409572

(41) Weng, Q.-H.; Hu, M.-H.; Wang, J.-F.; Hu, J.-J. Enhancing the Flexibility and Hydrophilicity of PLA via Polymer Blends: Electrospinning vs. Solvent Casting. *Polymers* **2025**, *17* (6), 800. https://doi.org/10.3390/polym17060800

(42) Zhou, H.; Green, T. B.; Joo, Y. L. The Thermal Effects on Electrospinning of Polylactic Acid Melts. *Polymer* **2006**, *47* (21), 7497–7505. https://doi.org/10.1016/j.polymer.2006.08.042

(43) Vadas, D.; Nagy, Z. K.; Csontos, I.; Marosi, G.; Bocz, K. Effects of Thermal Annealing and Solvent-Induced Crystallization on the Structure and Properties of Poly(Lactic Acid) Microfibres Produced by High-Speed Electrospinning. *J. Therm. Anal. Calorim.* **2020**, *142* (2), 581–594. https://doi.org/10.1007/s10973-019-09191-8

(44) Yan, J.; Zheng, Y.; Zhou, Y.; Liu, Y.; Tan, H.; Fu, Q.; Ding, M. Application of Infrared Spectroscopy in the Multiscale Structure Characterization of Poly(l-Lactic Acid). *Polymer* **2023**, *278*, 125985. https://doi.org/10.1016/j.polymer.2023.125985

(45) Siriprom, W.; Sangwaranatee, N.; Herman; Chantarasunthon, K.; Teanchai, K.; Chamchoi, N. Characterization and Analyzation of the Poly (L-Lactic Acid) (PLA) Films. *Mater. Today Proc.* **2018**, *5* (7, Part 1), 14803–14806. https://doi.org/10.1016/j.matpr.2018.04.009

(46) Makreski, P.; Pejov, L.; Jovanovski, G. Crossroads of Vibrational (Infrared and Raman) Spectroscopy and X-Ray Powder Diffraction in Identification and Characterization of Some Minerals – Advantages and Limitations. A Review. *Maced. J. Chem. Chem. Eng.* **2024**, *43* (1), 1–28. https://doi.org/10.20450/mjcce.2024.2858

(47) Karatas, M. Removal of Pb(II) from Water by Natural Zeolitic Tuff: Kinetics and Thermodynamics. *J. Hazard. Mater.* **2012**, *199–200*, 383–389. https://doi.org/10.1016/j.jhazmat.2011.11.035

(48) Varshney, D.; Kumar, A. Structural and Optical Properties of Ni Substituted $CaCu_3Ti_4 - xNi_xO_{12}$. *Optik* **2015**, *126* (22), 3437–3441. https://doi.org/10.1016/j.ijleo.2015.06.069

(49) Dai, Y.; Niu, L.; Zou, J.; Chen, T.; Liu, H.; Zhou, Y. Preparation of Core-Shell Magnetic Fe_3O_4@SiO_2-Dithiocarbamate Nanoparticle and Its Application for the Ni^{2+}, Cu^{2+} Removal. *Chin. Chem. Lett.* **2018**, *29* (6), 887–891. https://doi.org/10.1016/j.cclet.2017.11.029

(50) Ye, R.-P.; Gong, W.; Sun, Z.; Sheng, Q.; Shi, X.; Wang, T.; Yao, Y.; Razink, J. J.; Lin, L.; Zhou, Z.; Adidharma, H.; Tang, J.; Fan, M.; Yao, Y.-G. Enhanced Stability of Ni/SiO2 Catalyst for CO2 Methanation: Derived from Nickel Phyllosilicate with Strong Metal-Support Interactions. *Energy* **2019**, *188*, 116059. https://doi.org/10.1016/j.energy.2019.116059

(51) Lee, J.-Y.; Chen, C.-H.; Cheng, S.; Li, H.-Y. Adsorption of Pb(II) and Cu(II) Metal Ions on Functionalized Large-Pore Mesoporous Silica. *Int. J. Environ. Sci. Technol.* **2016**, *13* (1), 65–76. https://doi.org/10.1007/s13762-015-0841-y

(52) Ali, A.; Alharthi, S.; Ahmad, B.; Naz, A.; Khan, I.; Mabood, F. Efficient Removal of Pb(II) from Aqueous Medium Using Chemically Modified Silica Monolith. *Molecules* **2021**, *26* (22), 6885. https://doi.org/10.3390/molecules26226885

(53) Stein, M.; Buchweitz, M.; Mayer, P.; Rennert, T. Does Adsorption of Cd, Cu and Pb on Polymeric Silicic Acid Occur Under Acidic Conditions? *Silicon* **2023**, *15* (16), 7205–7212. https://doi.org/10.1007/s12633-023-02576-3

(54) Ren, J.; Zheng, L.; Su, Y.; Meng, P.; Zhou, Q.; Zeng, H.; Zhang, T.; Yu, H. Competitive Adsorption of Cd(II), Pb(II) and Cu(II) Ions from Acid Mine Drainage with Zero-Valent Iron/Phosphoric Titanium Dioxide: XPS Qualitative Analyses and DFT Quantitative Calculations. *Chem. Eng. J.* **2022**, *445*, 136778. https://doi.org/10.1016/j.cej.2022.136778

(55) Du, J.; Fan, L.; Wang, Q.; Min, F. Adsorption of Cr(OH)n(3−n) + (n = 1–3) on Illite (001) and (010) Surfaces: A DFT Study. *Processes* **2021**, *9* (11), 2048. https://doi.org/10.3390/pr9112048

(56) Bao, J.; Feng, Y.; Pan, Y.; Jiang, J. Adsorption of Co2+ and Cr3+ in Industrial Wastewater by Magnesium Silicate Nanomaterials. *Materials* **2024**, *17* (9), 1946. https://doi.org/10.3390/ma17091946

(57) Fijoł, N.; Abdelhamid, H. N.; Pillai, B.; Hall, S. A.; Thomas, N.; Mathew, A. P. 3D-Printed Monolithic Biofilters Based on a Polylactic Acid (PLA) – Hydroxyapatite (HAp) Composite for Heavy Metal Removal from an Aqueous Medium. *RSC Adv.* **2021**, *11* (51), 32408–32418. https://doi.org/10.1039/D1RA05202K

(58) Chen, J.; Duan, Q.; Liu, J.; Zhang, S.; Zhang, J.; Lin, S. Adsorption of Fe-Modified Peanut Shell Biochar for Pb(II) in Mixed Pb(II), Cu(II), Ni(II) Solutions. *Sci. Rep.* **2025**, *15* (1), 13558. https://doi.org/10.1038/s41598-025-97042-y

(59) Prazeres Mazur, L.; Reis Ferreira, R.; Felix da Silva Barbosa, R.; Henrique Santos, P.; Barcelos da Costa, T.; Gurgel Adeodato Vieira, M.; Da Silva, A.; Dos Santos Rosa, D.; Helena Innocentini Mei, L. Development of Novel Biopolymer Membranes by Electrospinning as Potential Adsorbents for Toxic Metal Ions Removal from Aqueous Solution. *J. Mol. Liq.* **2024**, *395*, 123782. https://doi.org/10.1016/j.molliq.2023.123782